This article was downloaded by:
On: *25 January 2011*
Access details: *Access Details: Free Access*
Publisher *Taylor & Francis*
Informa Ltd Registered in England and Wales Registered Number: 1072954 Registered office: Mortimer House, 37-41 Mortimer Street, London W1T 3JH, UK

Separation Science and Technology
Publication details, including instructions for authors and subscription information:
http://www.informaworld.com/smpp/title~content=t713708471

Preparation and Characterization of Titanium Dioxide (TiO_2) from Sludge produced by $TiCl_4$ Flocculation with $FeCl_3$, $Al_2(SO_4)_3$ and $Ca(OH)_2$ Coagulant Aids in Wastewater

H. K. Shon[a]; S. Vigneswaran[a]; J. Kandasamy[a]; M. H. Zareie[a]; J. B. Kim[b]; D. L. Cho[b]; J. -H. Kim[b]
[a] Faculty of Engineering Science, University of Technology, Sydney, Broadway, Australia [b] School of Applied Chemical Engineering & Center for Functional Nano Fine Chemicals, Chonnam National University, Gwangju, Korea

To cite this Article Shon, H. K. , Vigneswaran, S. , Kandasamy, J. , Zareie, M. H. , Kim, J. B. , Cho, D. L. and Kim, J. -H.(2009) 'Preparation and Characterization of Titanium Dioxide (TiO_2) from Sludge produced by $TiCl_4$ Flocculation with $FeCl_3$, $Al_2(SO_4)_3$ and $Ca(OH)_2$ Coagulant Aids in Wastewater', Separation Science and Technology, 44: 7, 1525 — 1543
To link to this Article: DOI: 10.1080/01496390902775810
URL: http://dx.doi.org/10.1080/01496390902775810

PLEASE SCROLL DOWN FOR ARTICLE

Full terms and conditions of use: http://www.informaworld.com/terms-and-conditions-of-access.pdf

This article may be used for research, teaching and private study purposes. Any substantial or systematic reproduction, re-distribution, re-selling, loan or sub-licensing, systematic supply or distribution in any form to anyone is expressly forbidden.

The publisher does not give any warranty express or implied or make any representation that the contents will be complete or accurate or up to date. The accuracy of any instructions, formulae and drug doses should be independently verified with primary sources. The publisher shall not be liable for any loss, actions, claims, proceedings, demand or costs or damages whatsoever or howsoever caused arising directly or indirectly in connection with or arising out of the use of this material.

Separation Science and Technology, 44: 1525–1543, 2009
Copyright © Taylor & Francis Group, LLC
ISSN: 0149-6395 print/1520-5754 online
DOI: 10.1080/01496390902775810

Taylor & Francis
Taylor & Francis Group

Preparation and Characterization of Titanium Dioxide (TiO_2) from Sludge produced by $TiCl_4$ Flocculation with $FeCl_3$, $Al_2(SO_4)_3$ and $Ca(OH)_2$ Coagulant Aids in Wastewater

H. K. Shon,[1] S. Vigneswaran,[1] J. Kandasamy,[1] M. H. Zareie,[1] J. B. Kim,[2] D. L. Cho,[2] and J.-H. Kim[2]

[1]Faculty of Engineering Science, University of Technology, Sydney, Broadway, Australia

[2]School of Applied Chemical Engineering & Center for Functional Nano Fine Chemicals, Chonnam National University, Gwangju, Korea

Downloaded At: 09:02 25 January 2011

Abstract: In this study, $TiCl_4$ coagulant together with coagulant aids such as $FeCl_3$, $Al_2(SO_4)_3$, and $Ca(OH)_2$ were investigated to improve the photoactivity of titanium dioxide (TiO_2) produced from sludge and to increase the resulting low pH value. After $TiCl_4$ flocculation with three coagulant aids, the settled floc (sludge) was incinerated at 600°C to produce TiO_2 doped with Fe, Al, and Ca elements. Fe-, Al-, and Ca-doped TiO_2 was characterized in terms of structural, chemical, and photo-electronic properties. All the coagulant aids used together with Ti-salt flocculation effectively increased the pH values. The surface area of TiO_2-WO (without any coagulant aids), Fe/TiO_2, Al/TiO_2, and Ca/TiO_2 was 122 m^2/g, 77 m^2/g, 136 m^2/g and 116 m^2/g, respectively. The TiO_2-WO, Fe/TiO_2, Al/TiO_2, and Ca/TiO_2 was found to be of anatase phase. The XRD pattern on the Fe/TiO_2 included an additional peak of hematite (α-Fe_2O_3). The majority of gaseous acetaldehyde with TiO_2-WO and Ca/TiO_2 for photocatalytic activity was completely removed within 40 minutes under UV irradiation.

Keywords: Flocculation, recycle, titanium dioxide (TiO_2), wastewater

Received 23 August 2008; accepted 20 December 2008.

Address correspondence to H. K. Shon, Faculty of Engineering Science, University of Technology, Sydney, P.O. Box 123 Sydney, Broadway, NSW 2007, Australia. Tel.: +612 95142629; Fax: +612 95142633. E-mail: hkshon@eng.uts.edu.au

INTRODUCTION

Sludge disposal is one of the major problems in sewage treatment plants (STP). Chemical flocculation produces a large amount of sludge (settled floc) which is generally disposed of in landfills. However, landfills are becoming less acceptable in view of growing community resistance. An appropriate method of efficient sludge recycling is thus required. Flocculation of wastewater with Ti-salt and production of TiO_2 from flocculated sludge was investigated (1). This work used titanium tetrachloride ($TiCl_4$) as an alternative coagulant instead of more commonly used salts of iron ($FeCl_3$) and aluminium ($Al_2(SO_4)_3$) to remove organic matter from wastewater. The alternative coagulant ($TiCl_4$) successfully removed organic matter and nutrients (phosphorus) to the same extent as Fe and Al salts. The floc size of the settled floc with the titanium salt was bigger than that of the Fe and Al salts and this led to faster and more effective settling. After flocculation with titanium salt, the settled floc was incinerated to produce functional TiO_2, which had the same qualities as that of commercial TiO_2. The TiO_2 was found to be mainly doped with C- and P-atoms. The atomic percentage of the TiO_2 was $TiO_{1.42}C_{0.44}P_{0.14}$. This results in an efficient and economical process not only in terms of removal of organic matter, but also reduction of the large amount of sludge that requires disposal. The amount of TiO_2 recovered by this process from STP can potentially meet the current demand of TiO_2 used in all major applications. However, the treated water after flocculation had the low pH.

The pH value of the supernatant at the optimum concentration of 8.4 Ti-mg/L of $TiCl_4$ flocculation was very low (pH 3.25), and was much lower than those of Fe and Al salt flocculation (1). The problem could be solved by post-treatment after $TiCl_4$ flocculation. The post-treatment could be an addition of sodium hydroxide (NaOH) to neutralize the pH value. Alternatively, coagulant aids such as $FeCl_3$, $Al_2(SO_4)_3$, and $Ca(OH)_2$ could be simultaneously added during flocculation with $TiCl_4$. Incineration of co-flocculated sludge would produce Fe-, Al- and Ca-doped TiO_2.

TiO_2 is the most widely used metal oxide for environmental applications, cosmetics, paints, electronic paper, and solar cells (2–4). Metal ions have been widely used as dopants to improve the photocatalytic efficiency of TiO_2. As metal ions are doped into TiO_2, impurity energy levels in the band gap are formed. This leads to an alteration of the electron hole recombination. Metals are either deposited or doped on the TiO_2 surfaces as metallic nanoparticles or as ionic dopants. Fe-doped TiO_2 improved photocatalytic activity under visible light irradiation (5,6). Fe^{3+} cations acted as shallow traps in the TiO_2 lattice. Fe ions trapped

Downloaded At: 09:02 25 January 2011

not only electrons but also holes, which led to an increase in photoactivity (7). The maximum photoactivity appeared with 0.5 wt.% of Fe^{3+} due to a decrease in the density of the surface active centres (8). Al-doped TiO_2 has been used for potential thermal shock applications due to its stable thermal expansion coefficient and physical property (9). Al_2O_3 and Al_2TiO_5 were observed at $AlCl_3/TiCl_4$ ratios larger than 1.1 at 1400°C (10). They found that a new structure connected with Al-O-Ti framework was generated. For Al/TiO_2, the anatase structure was stable after incineration at 800°C, while pure TiO_2 was easily transferred to the rutile phase after incineration above 700°C. The optical property of Al/TiO_2 prepared by a thermal plasma method responded to visible light (11). They also found that the size of the synthesized powder decreased with an increase in the amount of Al because Al species inhibited the particle growth. Al/TiO_2 has been applied as a gas sensor, which needs high conductivity of TiO_2 (12). Ca-doped TiO_2 is an important material known for its use in ferroelectric ceramics, communication equipment for microwave frequencies, and a host matrix for the fixation of lanthanides and actinides for the immobilization of high-level radioactive wastes (13,14). $CaTiO_3$ has high dielectric loss, is a thermally-sensitive resistor element due to its negative temperature coefficient and is a refractory material with high corrosion receptivity against caustic solutions. The compound is mostly synthesized by

1. a solid state reaction between $CaCO_3$ or CaO and TiO_2 at 1350°C,
2. sol-gel processing,
3. thermal deposition of peroxo-salts, and
4. mechano-chemical synthesis.

In this study, we tried to improve photoactivity TiO_2 produced from sludge and to increase the low pH after $TiCl_4$ flocculation by the use of coagulant aids. The $TiCl_4$ coagulant was added with coagulant aids such as $FeCl_3$, $Al_2(SO_4)_3$ and $Ca(OH)_2$. The flocculation produced Fe/TiO_2, Al/TiO_2, and Ca/TiO_2. The metal-doped TiO_2 was characterized in terms of structural, chemical and photo-electronic properties.

EXPERIMENTAL

Organic Removal by $TiCl_4$ Flocculation with Coagulant Aids in Synthetic Wastewater

Flocculation of synthetic wastewater was carried out with $TiCl_4$ (2.1 – 8.4 Ti-mg/L) together with different doses of coagulant aids of $FeCl_3$

Downloaded At: 09:02 25 January 2011

(3.4–13.8 Fe-mg/L), $Al_2(SO_4)_3$ (4.0–16.0 Al-mg/L), and $Ca(OH)_2$ (5–15 Ca-mg/L). The composition of the synthetic wastewater is presented elsewhere (15). This synthetic wastewater represents the biologically-treated sewage effluent. Tannic acid, peptone, sodium lignin sulfornate, sodium lauryle sulfate, and arabic acid represent the larger molecular weight portion, while peptone, beef extract, and humic acid comprise the organic matters of lower molecular weight (16). The wastewater with $TiCl_4$ coagulant and coagulant aids was stirred rapidly for 1 minute at 100 rpm, followed by 20 minutes of slow mixing at 30 rpm, and 30 minutes of settling. Organic matter in terms of dissolved organic carbon (DOC) was measured using a Dohrmann Phoenix 8000 UV-persulphate TOC analyzer equipped with an autosampler. All samples were filtered through 0.45 μm membrane prior to organic measurement. The pH was measured using a pH meter (Orion, model 920A).

Downloaded At: 09:02 25 January 2011

Characterization of TiO_2

Visual microscopy was used to measure the shape and aggregated particle size of TiO_2. Scanning electron microscopy/energy dispersive X-ray (SEM/EDX, Rigaku, Japan) and a Digital Instruments Multimode Nanoscope III scanning force microscope were used. Each imaging was conducted in tapping mode, with 512×512 data acquisitions at a scan speed of 1.4 Hz at room temperature in air. Oxide-sharpened silicon nitride tips with integrated cantilevers with a nominal spring constant of 0.38 N/m were used for atomic force microscopy (AFM). The roughness of the particles was assessed by measuring the roughness parameters.

Nitrogen adsorption–desorption isotherms were recorded using a ASAP 2020 model (Micromeritics Ins., USA) and the specific surface areas were determined by the Brunauer–Emmett–Teller (BET) method. X-ray diffraction (XRD) images (Rigaku, Japan) of anatase and rutile TiO_2 photocatalysts were investigated to identify the particle structure. All the XRD patterns were analyzed with MDI Jade 5.0 (Materials Data Inc., USA). The crystallite size of powders was determined from the broadening of corresponding XRD peaks by Scherrer's formula. UV-VIS-NIR spectrophotometer (Cary 500 Scan, Varian, USA) was used to identify the absorbance range. The photocatalytic activity test of TiO_2 was investigated under UV irradiation (Sankyo, F10T8BLB, three 10 W lamps) and visible light (Kumbo, FL10D, three 10 W lamps) using the method of photodecomposition of gaseous acetaldehyde. The concentration of acetaldehyde was measured by gas chromatography with flame ionization detector (Youngin, M600D, Korea).

RESULTS AND DISCUSSION

DOC Removal and pH Variation by $TiCl_4$ with Coagulant Aids

DOC removal and pH variation after flocculation of synthetic wastewater at different $TiCl_4$ concentrations were studied. At 8.4 Ti-mg/L (the optimum concentration), the DOC removal and pH were 70% and pH 3.25, respectively. To increase the pH value, the use of coagulant aids $FeCl_3$, $Al_2(SO_4)_3$ and $Ca(OH)_2$ with $TiCl_4$ was explored.

Table 1 presents DOC removal and pH variation with different concentrations of $TiCl_4$ and $FeCl_3$ coagulant aid. Here, the optimum concentrations were chosen by the measured turbidity and DOC removal. When the turbidity value of the effluent after flocculation was less than 2 NTU, the optimum concentration was considered.

The optimum concentration of Ti and Fe salts was 4.2 Ti-mg/L and 6.9 Fe-mg/L, respectively. The pH value and DOC removal at the optimum concentration of Ti and Fe salts were 4.7 and 70%, respectively. DOC removal and pH were also studied with different concentrations of $TiCl_4$ and $Al_2(SO_4)_3$ (Table 2). The optimum concentration of Ti and Al salts was 4.2 Ti-mg/L and 8.0 Al-mg/L, respectively. The pH value and DOC removal at the optimum concentration of Ti- and Al-salt were 4.5 and 72%, respectively. Table 3 shows DOC removal and pH variation with different concentrations of $TiCl_4$ and $Ca(OH)_2$ in synthetic wastewater. The optimum concentration of Ti- and Ca-salts was 6.3

Downloaded At: 09:02 25 January 2011

Table 1. DOC removal and pH variation with different concentrations of $TiCl_4$ and $FeCl_3$ in synthetic wastewater (initial concentration of DOC = 10.05 mg/L; initial pH of synthetic wastewater before the addition of $TiCl_4$ = 7.3)

Ti concentration (Ti-mg/L)	Al concentration (Al-mg/L)	pH	DOC removal (%)
2.1	4.0	4.8	53
	8.0	4.7	55
	16.0	4.5	58
4.2	4.0	4.7	65
	8.0	4.5	72
	16.0	4.1	72
6.3	4.0	4.1	65
	8.0	4.1	73
	16.0	3.9	75
8.4	4.0	3.2	75
	8.0	3.1	75
	16.0	3.0	75

Table 2. DOC removal and pH variation with different concentrations of $TiCl_4$ and $Al_2(SO_4)_3$ in synthetic wastewater (initial concentration of DOC = 10.05 mg/L; initial pH = 7.3)

Ti concentration (Ti-mg/L)	Al concentration (Al-mg/L)	pH	DOC removal (%)
2.1	4.0	4.8	53
	8.0	4.7	55
	16.0	4.5	58
4.2	4.0	4.7	65
	8.0	4.5	72
	16.0	4.1	72
6.3	4.0	4.1	65
	8.0	4.1	73
	16.0	3.9	75
8.4	4.0	3.2	75
	8.0	3.1	75
	16.0	3.0	75

Ti-mg/L and 15.0 Ca-mg/L, respectively. The pH value and DOC removal at the optimum concentration of Ti and Ca were 7.6 and 70%, respectively.

All the three coagulant aids increased the pH value. The Fe- and Al-salt coagulants aids increased the pH range only by a small amount

Table 3. DOC removal and pH variation with different concentrations of $TiCl_4$ and $Ca(OH)_2$ in synthetic wastewater (initial concentration of DOC = 10.05 mg/L; initial pH = 7.3)

Ti concentration (Ti-mg/L)	Ca concentration (Ca-mg/L)	pH	DOC removal (%)
2.1	5	7.8	40
	10	8.2	45
	15	8.9	50
4.2	5	7.7	53
	10	8.0	55
	15	8.7	59
6.3	5	6.3	63
	10	7.2	65
	15	7.6	70
8.4	5	6.1	72
	10	6.7	73
	15	7.8	75

Downloaded At: 09:02 25 January 2011

(about pH 5), while the Ca-salt coagulant significantly increased the pH (close to neutral pH value). This is due to the input of OH^- ions from $Ca(OH)_2$. The DOC removal increased with the increase in concentration of the coagulant aids. The DOC removal was 70% to 72% for Fe and Al salt concentration of 6.9 Fe-mg/L and 8 Al-mg/L, respectively. Ca-salt concentration of 15 Ca-mg/L achieved DOC removal of 70%. This can be explained in terms of the charge of the cations. The higher the charge of a cation, the stronger is its effect on the zeta-potential. The higher the valance, the higher the coagulative power (17,18). Here, the coagulative power is defined as "the given volume of colloidal solution added to a quantity of electrolyte just sufficient to produce coagulation of the particles."

To investigate the properties of TiO_2 obtained from flocculation sludge, the settled flocs after flocculation were collected and incinerated at 600°C. TiO_2 without any coagulant aids is called as TiO_2-WO in this study. TiO_2 obtained from $TiCl_4$ coagulant together with Fe-, Al-, and Ca-salt coagulant aids at the different optimum concentrations are hereafter expressed as Fe/TiO_2, Al/TiO_2 and Ca/TiO_2, respectively.

Downloaded At: 09:02 25 January 2011

Surface Area of TiO_2-WO, Fe/TiO_2, Al/TiO_2, and Ca/TiO_2

N_2 adsorption–desorption isotherms were used to investigate the surface area, average pore diameter and pore volume of TiO_2-WO, Fe/TiO_2, Al/TiO_2 and Ca/TiO_2 (Fig. 1a). Table 4 summarizes the results of the surface area, average pore diameter, and pore volume of TiO_2-WO, Fe/TiO_2, Al/TiO_2 and Ca/TiO_2. The BET specific surface area of all the TiO_2 (produced in this study) was higher than that of the P-25 TiO_2 ($50\,m^2/g$) which is the most widely used photocatalyst (19). The surface area of Fe/TiO_2 was lower than that of TiO_2-WO. Previous studies also found a lower surface area for Fe/TiO_2 (20–22). Adan et al. (20) observed an appreciably lower surface area and mesopore volume at 0.7–1.5 wt.% of iron content. This correlates with the attainment of the solubility limit for Fe^{3+} ions into the TiO_2 structure and could be related to the onset of the generation of some iron aggregates at the TiO_2 surface. In contrast, Neri et al. (23) found that by increasing the Fe content, the BET surface area was significantly increased, showing a maximum ($49.5\,m^2/g$) for the sample with 50 wt.%–Fe/Ti.

The surface area of Al/TiO_2 showed the highest values ($136.0\,m^2/g$). This may be due to a porous structure of Al-O-Ti (10). Choi et al. (12) reported that an increase in Al dopant concentration up to 5 wt.% resulted in an increase in crystallite size. This size decreased at 7.5 wt.% Al. Lee et al. (10) reported that with the increase of the Al dopant,

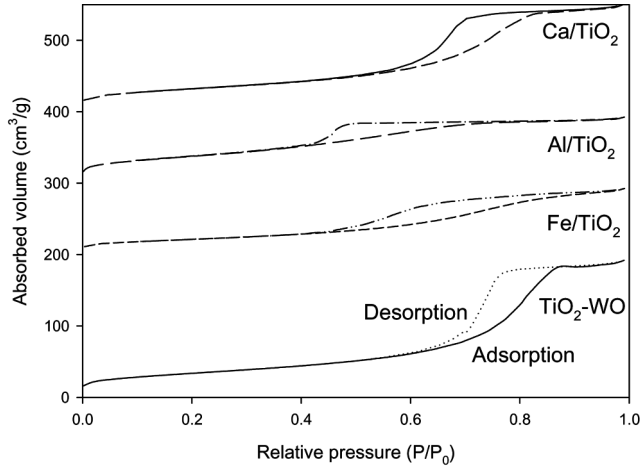

(a) N_2 adsorption–desorption isotherms

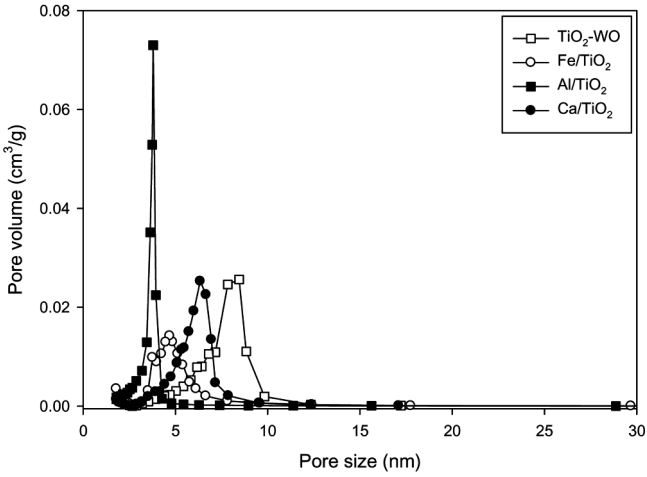

(b) Pore size distribution

Figure 1. (a) N_2 adsorption–desorption isotherms and (b) pore size distribution of incinerated TiO_2-WO, Fe/TiO_2, Al/TiO_2, and Ca/TiO_2.

the size of TiO_2 particles decreased due to the suppression of particle growth by an introduction of Al atoms into TiO_2 crystal. The surface area of Ca/TiO_2 was similar to that of TiO_2-WO.

Figure 1 (b) and Table 4 show the average pore diameter and pore size distribution. The intra-particle pore size and volume were measured as the pore size distribution of incinerated TiO_2-WO, Fe/TiO_2, Al/TiO_2, and Ca/TiO_2 as calculated by the Barrett–Joyner–Halenda method (24)

Downloaded At: 09:02 25 January 2011

Table 4. Surface area, average pore diameter and pore volume of TiO_2-WO, Fe/TiO_2, Al/TiO_2 and Ca/TiO_2

	Surface area (m^2/g)	Average pore diameter (nm)	Pore volume (cm^3/g)
TiO_2-WO	122.0	9.7	0.30
Fe/TiO_2	76.8	7.4	0.14
Al/TiO_2	136.0	4.2	0.14
Ca/TiO_2	115.7	8.0	0.23

showed less than 10 nm. Yu et al. (25) reported that biomodal pore size distribution consists of small intra-particle pores (4–10 nm) and larger inter-particle pores (20–200 nm). The average pore diameter decreased in the following order: TiO_2-WO > Ca/TiO_2 > Fe/TiO_2 > Al/TiO_2. The pore volume also decreased in the following order: TiO_2-WO > Ca/TiO_2 > $Fe/TiO_2 = Al/TiO_2$.

Downloaded At: 09:02 25 January 2011

XRD Results

Figure 2 presents the XRD patterns of TiO_2-WO, Fe/TiO_2, Al/TiO_2, and Ca/TiO_2 incinerated at 600°C. The XRD patterns were made to identify

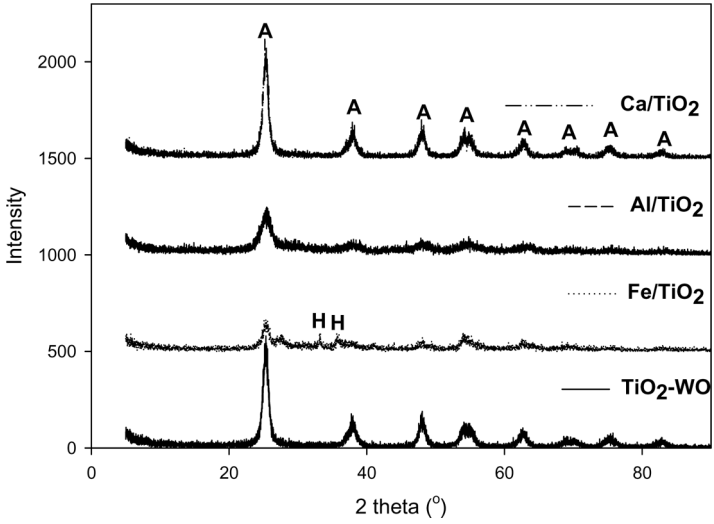

Figure 2. XRD patterns of TiO_2-WO, Fe/TiO_2, Al/TiO_2, and Ca/TiO_2 produced from incineration of the settled floc at 600°C (A: anatase phase (TiO_2); H: hematite (α-Fe_2O_3)).

the particle structure and size. The TiO_2-WO, Fe/TiO_2, Al/TiO_2, and Ca/TiO_2 exhibited the majority of the anatase phase. The XRD pattern on the Fe/TiO_2 showed a peak of hematite (α-Fe_2O_3). The peak of low intensity, due to an iron-TiO_2 mixed phase, of composition Fe_2TiO_5, crystallized poorly in very small grain sizes evidenced by the remarkable enlargement of the diffraction peak, as detected on the Fe/TiO_2. Neri et al. (23) reported that for iron content >50%, the XRD patterns showed only the strong reflections of α-Fe_2O_3, whose intensity increased with a larger Fe content. The pattern on the Fe/TiO_2 also suggests a decrease of crystallinity compared with other TiO_2. This may be due to high iron concentration. In contrast, Zhang et al. (26) demonstrated that when iron concentration was less than 10 wt.%, the TiO_2 was all in anatase phase and there was no peak of iron oxide in the XRD patterns.

A crystalline phase containing Al atoms (α-Al_2O_3 and Al_2TiO_5) was not observed in the Al/TiO_2. This is due to low concentrations of Al_2O_3 and/or a substitute site (Al^{3+}) for a Ti^{4+} ion (26). Since the ionic radius for Al and Ti are similar (0.68 Å for Al^{3+}), Al can occupy a regular cation position, forming a substitutional solid solution. In addition, Al species dissolve well into the TiO_2 crystal (11). The crystalline phase containing Ca atoms (CaO and $CaTiO_3$) was not observed on the Ca/TiO_2. To sum up, different crystalline phases such as α-Al_2O_3 and Al_2TiO_5 from Al/TiO_2 and CaO and $CaTiO_3$ from Ca/TiO_2 were not found. On the other hand, the XRD pattern of α-Fe_2O_3 from Fe/TiO_2 was observed.

The crystalline size of different TiO_2 was calculated using Scherrer's formula (28). The crystallite size of TiO_2-WO, Fe/TiO_2, Al/TiO_2, and Ca/TiO_2 was approximately 11 nm, 6 nm, 8 nm, and 11 nm, respectively. The intensity of the anatase phase on Fe/TiO_2 and Al/TiO_2 significantly decreased. This suggests that the Fe and Al species inhibited a crystalline growth (11). On the other hand, the intensity of the anatase phase on the Ca/TiO_2 was similar to that on the TiO_2-WO.

SEM/EDX Results

Figure 3 shows the SEM images and EDX spectra of TiO_2-WO, Fe/TiO_2, Al/TiO_2, and Ca/TiO_2. The SEM images of TiO_2-WO, Fe/TiO_2, Al/TiO_2, and Ca/TiO_2 consisted of a different size, shape, and dimension of the particles. The majority of the particles were found to be less than 1 μm, which were constituted by aggromerates of 0.05 μm particles. The SEM image of Fe/TiO_2 particles included very irregular shape and smaller dimensions of 0.1 μm size compared to other particles observed by SEM images of TiO_2-WO, Al/TiO_2 and Ca/TiO_2. Navio et al. (22) reported that Fe/Ti samples (less than 3 wt.% Fe) gave deposits irregular

Downloaded At: 09:02 25 January 2011

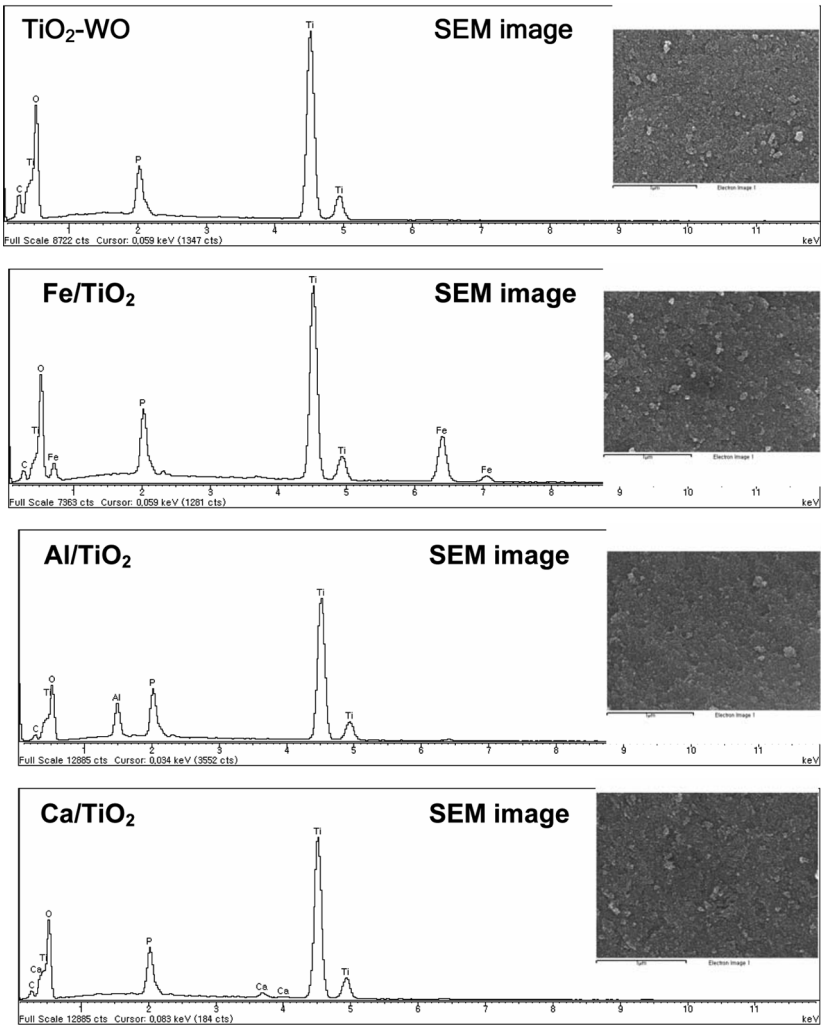

Figure 3. EDX spectra and SEM images of TiO_2-WO, Fe/TiO_2, Al/TiO_2, and Ca/TiO_2 nanoparticles.

in shape and dimensions, while the Fe/Ti samples (more than 5 wt.% Fe) showed deposits homogeneous in shape and dimensions. Adan et al. (20) reported that the presence of iron in the samples apparently affected the particle size. A maximum effect on the particle size is observed at around 1 wt.% doping level. The SEM image of Al/TiO_2 particles indicated that the size of the irregular shape and dimensions in Al/TiO_2 were smaller than those in Fe/TiO_2. Lee et al. (11) reported that with the increase

Downloaded At: 09:02 25 January 2011

Table 5. Atomic (%) fraction of TiO_2-WO, Fe/TiO_2, Al/TiO_2, and Ca/TiO_2 powders after incineration at 600°C

Element	TiO_2-WO	Fe/TiO_2	Al/TiO_2	Ca/TiO_2
Ti atomic %	20.9	18.1	20.7	20.4
O atomic %	65.6	64.3	65.3	67.2
C atomic %	10.9	8.2	7.8	8.3
P atomic %	2.7	2.9	2.7	3.7
Fe atomic %	–	6.52	–	–
Al atomic %	–	–	3.5	–
Ca atomic %	–	–	–	0.4

*Trace elements found in TiO_2-WO: Si (0.2%), Fe (0.02%), S (0.01%), Al (0.01%), V, Ca, Na, Cr, Cl, Ni, and Br.

Downloaded At: 09:02 25 January 2011

of Al dopant, the size of TiO_2 particles decreased due to the suppression of particle growth by an introduction of Al atoms into TiO_2 crystal.

EDX analysis was performed to determine the presence of the different elements in TiO_2-WO, Fe/TiO_2, Al/TiO_2 and Ca/TiO_2 (Fig. 3). EDX mapping technique showed that different elements were uniformly spread in/on TiO_2-WO, Fe/TiO_2, Al/TiO_2 and Ca/TiO_2. Table 5 shows the atomic fraction of different elements. The constitutive elements of TiO_2-WO were mainly Ti, O, C, and P, Fe/TiO_2 were mainly Fe, Ti, O, C, and P, Al/TiO_2 were mainly Al, Ti, O, C and P and Ca/TiO_2 were mainly Ca, Ti, O, C, P. Here, the C atom came from the remaining organic carbon of the settled organic matter. The P atom was from phosphorus nutrients present in wastewater. It is well known that flocculation removes the majority of organic matter and phosphorus from waste sludge (1). Most C and P atoms were doped as a substitute site for an O atom, while the Fe, Al, and Ca atoms were doped as a substitute site for a Ti atom (1,29). Although a relatively small amount of Fe concentration (6.9 Fe-mg/L) was added with $TiCl_4$ flocculation compared to Al (8.0 Al-mg/L) and Ca (15 Ca-mg/L) concentration, the atomic percentage of Fe, Al, Ca atoms in Fe/TiO_2, Al/TiO_2, and Ca/TiO_2 was 6.5%, 3.5%, and 0.4%, respectively. This suggests that flocculation of Ti-salt with Fe-salt coagulant was more favorable than with the Al- and Ca-salts.

Optical Absorbance

The optical property of TiO_2-WO, Fe/TiO_2, Al/TiO_2, and Ca/TiO_2 was investigated using the ultra violet–visible-near infrared (UV-VIS-NIR)

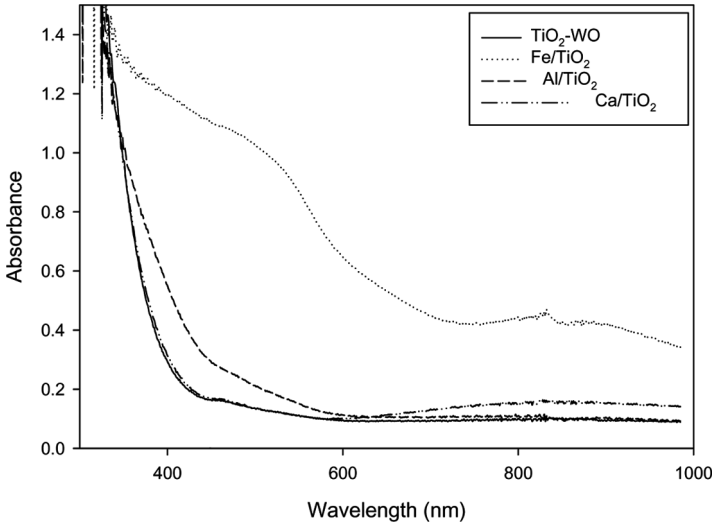

Figure 4. Optical absorbance of TiO_2-WO, Fe/TiO_2, Al/TiO_2, and Ca/TiO_2.

Downloaded At: 09:02 25 January 2011

spectrophotometer (Fig. 4). Generally, the absorption band of Ti^{4+} tetrahedral symmetry appears around 300 nm. The absorption bands of Fe/TiO_2 and Al/TiO_2 were significantly shifted to the visible range, while that of Ca/TiO_2 was not shifted. The red shift associated with the presence of Fe ions may be attributed to

1. a charge transfer transition between the Fe ion electrons and the TiO_2 conduction or valence band and/or
2. a dark reddish color with the increase of Fe concentration (30).

Swanepoel (31) found that the red shift of the absorption edge by Fe/TiO_2 was attributed to the excitation of 3d electrons of Fe^{3+} to the TiO_2 conduction band. When Al/TiO_2 was prepared using a thermal plasma method, the band edge of the powders shifted from UV region to visible light, suggesting that the shift of absorption spectrum was attributed to the band gap narrowing relating to the interstitial Al species in the TiO_2 crystal (11).

AFM Results

Figure 5 shows AFM images of TiO_2-WO, Fe/TiO_2, Al/TiO_2, and Ca/TiO_2 nanoparticles. Surface morphology of different nanoparticles

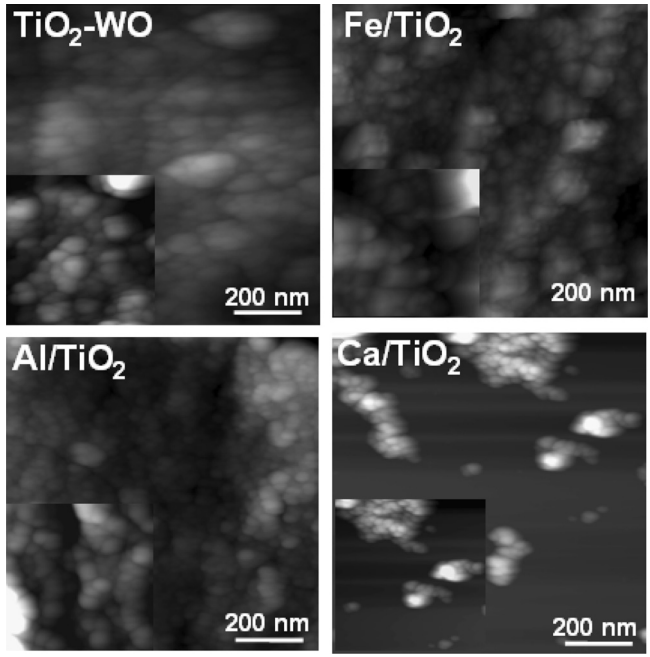

Figure 5. AFM images of TiO_2-WO, Fe/TiO_2, Al/TiO_2, and Ca/TiO_2 nanoparticles. All images are $1 \times 1\,\mu m$ and the insets in all images are $300 \times 300\,nm$.

Downloaded At: 09:02 25 January 2011

was determined using tapping mode AFM. TiO_2 powders prepared by the addition of different metals evidently consisted of a spherical shape and the size of the secondary particles was quite uniform. The results are contradictory to the previous finding (32). They reported that Al-doped TiO_2 had a positive ionic radius that was greatly different from Ti^{4+} and was not uniform due to severe agglomeration and had the larger secondary particle sizes. The image of Al/TiO_2 obtained in this study clearly shows the particles with different sizes from 34–80 nm. The variation of the sizes was observed in all images (TiO_2-WO, Fe/TiO_2, Al/TiO_2, and Ca/TiO_2). The higher resolution of this image is given in the inset with a scan area of $300 \times 300\,nm$. The shape features of Fe/TiO_2 particles consisted of particle size in the range of 33 to 70 nm. Ca/TiO_2 particles included the size from 18.9 nm to 39.7 nm. The crystalline particle size measured by AFM was different from that of XRD (measured using Scherrer's formula). This may be due to aggregation of particle as the secondary particles (33).

Table 6 presents the roughness values of TiO_2-WO, Fe/TiO_2, Al/TiO_2, and Ca/TiO_2 nanoparticles. The preparation method of TiO_2

Table 6. Roughness measurements of TiO_2-WO, Fe/TiO_2, Al/TiO_2 and Ca/TiO_2 nanoparticles (average roughness (S_a), root-mean-square roughness (S_q), surface area (S_{dr}), peak-peak count (S_y) and ten point height (S_z))

	S_a (nm)	S_q (nm)	S_{dr} (%)	S_y (nm)	S_z (nm)
TiO_2-WO	8.7	12.2	18.8	101.0	65.9
Fe/TiO_2	11.1	14.2	20.0	88.3	78.0
Al/TiO_2	8.1	10.3	13.1	59.9	54.0
Ca/TiO_2	9.6	12.1	45.5	83	62.7

produced in this manner was difficult to produce the TiO_2 thin film so that the aggregated particles were measured. This measurement of each roughness could be affected by the aggregated structure. They were measured in terms of average roughness (S_a), root-mean-square roughness (S_q), surface area (S_{dr}), peak-peak count (S_y), and ten-point height (S_z). Here, the peak-peak count is an estimate of the shape of the overall distribution of z-values which is short or wide and tall or narrow. The ten-point height is defined as the average height of the five highest local maximums plus the average height of the five lowest local minimums. The average roughness (S_a) of TiO_2-WO, Fe/TiO_2, Al/TiO_2, and Ca/TiO_2 was 8.7 nm, 11.1 nm, 8.1 nm and 9.6 nm, respectively. Sankapal et al. (31) also found that the root mean square roughness of 9 nm (which was calculated with contact mode for TiO_2 film).

Downloaded At: 09:02 25 January 2011

Photocatalytic Activity

The photocatalytic property of TiO_2-WO, Fe/TiO_2, Al/TiO_2, and Ca/TiO_2 was examined under irradiation of UV and visible light for the photodecomposition of gaseous acetaldehyde (Fig. 6). P-25 TiO_2 was used to compare the photocatalytic activity with other TiO_2. The concentration of acetaldehyde was measured by gas chromatography. The removal by adsorption showed the following order: Al/TiO_2 ($136\,m^2/g$) >> Ca/TiO_2 ($116\,m^2/g$) > TiO_2 ($122\,m^2/g$) > Fe/TiO_2 ($77\,m^2/g$) >= P-25 ($50\,m^2/g$). The majority of acetaldehyde with TiO_2-WO and Ca/TiO_2 was completely removed under UV irradiation within 40 minutes. P-25 TiO_2 and Al/TiO_2 led to a high photoactivity with the removal of 90%. However, at a high iron concentration (6.5 at.%), acetaldehyde removal by photo-oxidation under UV irradiation was marginal. Wang et al. (34) reported that the formation of Fe_2O_3 and Fe_2TiO_5 at high incineration temperature (600–800°C) resulted in a decrease of photocatalytic activity. Hung et al. (21) reported that the optimum

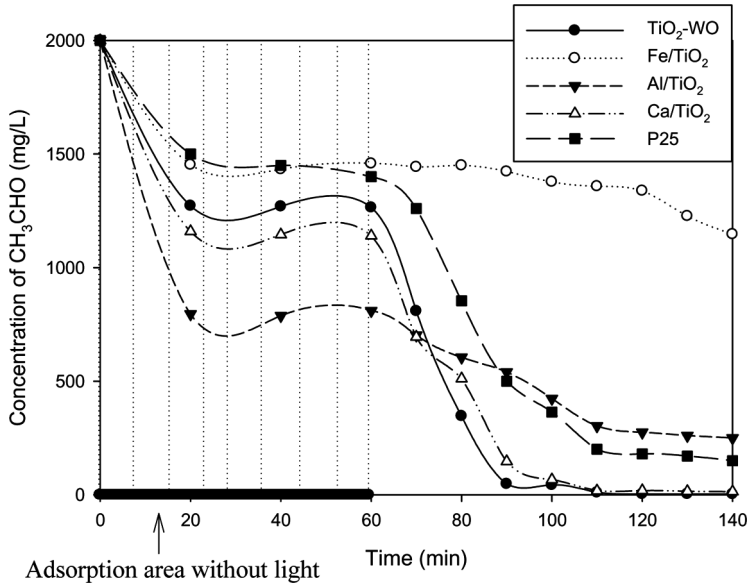

Figure 6. Variation of CH_3CHO concentration with UV irradiation time (TiO_2 concentration = 1 g; initial concentration of CH_3CHO = 2000 mg/L; UV irradiation = black light three 10 W lamps).

concentration of iron ions was 0.005% (Fe/Ti) and this enhanced gaseous dichloromethane removal. When the concentration of iron ions was high, the iron ions became recombination centers for the electron-hole pairs and reduced the photocatalytic activity. Under visible light, the photodecomposition of acetaldehyde using TiO_2-WO, Fe/TiO_2, Al/TiO_2, Ca/TiO_2, and P-25 was marginal.

CONCLUSIONS

$TiCl_4$ coagulant was added together with a predetermined quantity of coagulant aids such as $FeCl_3$, $Al_2(SO_4)_3$, and $Ca(OH)_2$ to improve photoactivity of TiO_2 increase the pH values after $TiCl_4$ flocculation. A detailed investigation was examined with Fe/TiO_2, Al/TiO_2 and Ca/TiO_2 produced from $TiCl_4$ co-flocculation. This led to the following conclusions:

1. All the coagulant aids helped to increase the pH values. The pH value and DOC removal at the optimum concentration of Ti and Fe salts were 4.7 and 70%, respectively as compared to 3.2 and 70% with $TiCl_4$

Downloaded At: 09:02 25 January 2011

without any coagulant aids. The pH value and DOC removal at the optimum concentration of Ti- and Al-salt were 4.5 and 72%, respectively. The pH value and DOC removal at the optimum concentration of Ti and Ca were 7.6 and 70%, respectively.

2. The surface area of TiO_2-WO, Fe/TiO_2, Al/TiO_2, and Ca/TiO_2 was 122 m^2/g, 77 m^2/g, 136 m^2/g and 116 m^2/g, respectively. The surface area was higher than that of P-25 (50 m^2/g).
3. TiO_2-WO, Fe/TiO_2, Al/TiO_2, and Ca/TiO_2 predominantly had anatase phase. However, the XRD pattern of the Fe/TiO_2 showed an additional peak of hematite (α-Fe_2O_3).
4. The SEM images of TiO_2-WO, Fe/TiO_2, Al/TiO_2, and Ca/TiO_2 consisted of different size, shape, and dimension of the particles. The majority of the particles were found to 0.05 μm. The average roughness of TiO_2-WO, Fe/TiO_2, Al/TiO_2 and Ca/TiO_2 was 8.7 nm, 11.1 nm, 8.1 nm and 9.6 nm, respectively.
5. The removal of acetaldehyde by adsorption was in good agreement with surface area of TiO_2-WO, Fe/TiO_2, Al/TiO_2, Ca/TiO_2, and P-25. With TiO_2-WO and Ca/TiO_2 as photocatalyst, the majority of acetaldehyde was completely removed under UV irradiation within 40 minutes. However, at a high iron concentration (6.5%), acetaldehyde removal was marginal. Under visible light, the photodecomposition of acetaldehyde using TiO_2-WO, Fe/TiO_2, Al/TiO_2, Ca/TiO_2, and P-25 was not identified.

Downloaded At: 09:02 25 January 2011

ACKNOWLEDGMENTS

This research was supported by UTS internal, CRC CARE, and Korea Research Foundation grants (KRF-2007-412-J02002).

REFERENCES

1. Shon, H.K.; Vigneswaran, S.; Kim, I.S.; Cho, J.; Kim, G.J.; Kim, J-.B.; Kim, J-.H. (2007) Preparation of functional titanium oxide (TiO_2) from sludge produced by titanium tetrachloride ($TiCl_4$) flocculation of wastewater. *Environ. Sci. Technol.*, *41*: 1372.
2. Kaneko, M., Okura, I. (2002) *Photocatalysis: Science and Technology*; Springer: Tokyo.
3. Jelks, B. (1966) *Titanium: Its Occurrence, Chemistry and Technology*; Ronald Press: New York.
4. Serpone, N.; Pelizzetti, E. (1989) *Photocatalysis: Fundamentals and Applications*; John Wiley & Sons: New York.

5. Teoh, W.Y.; Amal, R.; Madler, L.; Pratsinis, S.E. (2007) Flame sprayed visible light-active Fe-TiO_2 for photomineralisation of oxalic acid. *Catal. Today*, *120*: 203.
6. Liu, J.; Zheng, Z.; Zuo, K.; Wu, Y. (2006) Preparation and characterization of Fe^{3+}-doped Nanometer TiO_2 Photocatalysts. *Journal of Wuhan University of Technology (Materials Science Edition)*, *21*: 57.
7. Litter, M.I. (1999) Heterogeneous photocatalysis transition metal ions in photocatalytic systems. *Appl. Catal. B: Environ.*, *23*: 89.
8. Chatterjee, D.; Dasgupta, S. (2005) Visible light induced photocatalytic degradation of organic pollutants. *J. Photoch. Photobio.*, *6*: 186.
9. Li, C.; Shi, L.; Xie, D.; Du, H. (2006) Morphology and crystal structure of Al-doped TiO_2 nanoparticles synthesized by vapor phase oxidation of titanium tetrachloride. *J. Non-Cryst. Solids*, *352*: 4128.
10. Lee, B.Y.; Park, S.H.; Kang, M.; Lee, S.C.; Choung, S.J. (2003) Preparation of Al/TiO_2 nanometer photocatalyst film and the effect of H_2O addition on photocatalytic performance for benzene removal. *Appl. Catal. A: Gen.*, *253*: 371.
11. Lee, J.E.; Oh, S.M.; Park, D.W. (2004) Synthesis of nano-sized Al doped TiO_2 powders using thermal plasma. *Thin Solid Films.*, *457*: 230.
12. Choi, Y.J.; Seeley, Z.; Bandyopadhyay, A.; Bose, S.; Akbar, S.A. (2007) Aluminium-doped TiO_2 nano-powders for gas sensors. *Sensor. Actuat. B-Chem.*, *124*: 111.
13. Mi, G.; Murakami, Y.D.; Shindo, S. (1999) Mechnochemical synthesis of $CaTiO_3$ from a CaO-TiO_2 mixture and its HR-TEM observation. *Powder Technol.*, *105*: 162.
14. Brankovic, G.; Vutotic, V.Z.; Brankovic, J.A. (2007) Investigation on possibility of mechanochemical synthesis of $CaTiO_3$ from different precursors. *J. Eur. Ceram. Soc.*, *27*: 729.
15. Kim, S.H.; Shon, H.K.; (2007) Adsorption characterization for multi-component organic matters by titanium oxide (TiO_2) in Wastewater. *Sep. Sci. Technol.*, *42*: 1775–1792.
16. Shon, H.K.; Vigneswaran, S.; Ngo, H.H. (2005) Is semi-flocculation effective to ultrafiltration?. *Water Res.*, *39*: 147.
17. Mekhamer, W.K.; Assaad, F.F. (1999) Flocculation and coagulation of Ca- and K-saturated montmorillonite in the presence of polyethylene oxide. *J. Appl. Polym. Sci.*, *73*: 659.
18. Hunter, R.J. (1981) *Zeta Potential in Colloid Science Principles and Applications*; AP academic press: Sydney.
19. Asiltürk, M.; Sayılkan, F.; Erdemoğlu, S.; Akarsu, M.; Sayılkan, H.; Erdemoğlu, M.; Arpaç, E. (2006) Characterization of the hydrothermally synthesized nano-TiO_2 crystallite and the photocatalytic degradation of Rhodamine B. *J. Hazard. Mater.*, *129*: 164.
20. Adán, C.; Bahamonde, A.; Fernández-García, M.; Martínez-Arias, A. (2007) Structure and activity of nanosized iron-doped anatase TiO_2 catalysts for phenol photocatalytic degradation. *Appl. Catal. B: Environ.*, *72*: 11.

Downloaded At: 09:02 25 January 2011

21. Hung, W.C.; Fu, S.H.; Tseng, J.J.; Chu, H.; Ko, T.H. (2007) Study on photocatalytic degradation of gaseous dichloromethane using pure and iron ion-doped TiO_2 prepared by the sol–gel method. *Chemo.*, *66*: 2142.
22. Navio, J.A.; Colon, G.; Macias, M.; Real, C. (1999) Iron-doped titania semiconductor powders prepared by a sol-gel method. Part I: synthesis and characterization. *Appl. Catal. A: Gen.*, *177*: 111.
23. Neri, G.; Rizzo, G.; Galvagno, S.; Loiacono, G.; Donato, A.; Musolino, M.G.; Rombi, E. (2004) Sol-gel synthesis, characterization and catalytic properties of Fe-Ti mixed oxides. *Appl. Catal. A: Gen.*, *274*: 243.
24. Barrett, E.P.; Joyner, L.G.; Halenda, P.P. (1951) The determination of pore volume and area distributions in pure substances. *J. Am. Chem. Soc.*, *73*: 373.
25. Yu, J.G.; Yu, J.C.; Cheng, B.; Hark, S.K.; Iu, K. (2003) The effect of F^--doping and temperature on the structural and textural evolution of mesoporous TiO_2 powders. *J. Solid State Chem.*, *174*, 372.
26. Zhang, W.; Li, Y.; Zhu, S.; Wang, F. (2003) Surface modification of TiO_2 film by iron doping using reactive magnetron sputtering. *Chem. Phys. Lett.*, *373*: 333.
27. Kang, M. (2005) The superhydrophilicity of Al-TiO_2 nanometer sized material synthesized using a solvothermal method. *Mater. Lett.*, *59*: 3122.
28. Suryanarayana, C. (1995) Nanocrystalline materials. *Int. Mater. Rev.*, *40*: 41.
29. Yamashita, H.; Takeuchi, M.; Anpo, M. (2004) Visible-light-sensitive photocatlaysts. Encyclopedia of Nanoscience and Nanotechnology, UK.
30. Zhu, J.; Chen, F.; Zhang, J.; Chen, H.; Anpo, M. (2006) Fe^{3+}-TiO_2 photocatalysts prepared by combining sol–gel method with hydrothermal treatment and their characterization. *J. Photoch. Photobio. A.*, *180*: 196.
31. Swanepoel, R. (1983) Determination of the thickness and optical constants of amorphous silicon. *J. Physics E.*, *16*: 1214.
32. Hwang, D.S.; Lee, N.H.; Lee, D.Y.; Song, J.S.; Shin, S.H.; Kim, S.J. (2006) *Smart Mater. Struct.*, *15*: S74.
33. Sankapal, B.R.; Lux-Steiner, M.C.; Ennaoui, A. (2005) Phase transition control of nanostructured TiO_2 powders with additions of various metal chlorides. *Appl. Surf. Sci.*, *239*: 165.
34. Wang, Z.M.; Yang, G.; Biswas, P.; Bresser, W.; Boolchand, P. (2001) Processing of iron-doped titania powders in flame aerosol reactors. *Powder Technol.*, *114*: 197.

Downloaded At: 09:02 25 January 2011